第 33 卷第 2 期 无 机 化 学 学 报 Vol.33 No.2
2017 年 2 月 CHINESE JOURNAL OF INORGANIC CHEMISTRY 329-339

非血红素铁超氧化物活化丙烯分子多态反应机理的理论研究

吕玲玲*,[1] 朱元成[1] 左国防[1] 袁 焜[1] 王永成[2]
([1]天水师范学院化学工程与技术学院,天水 741001)
([2]西北师范大学化学化工学院,兰州 730070)

摘要: 采用密度泛函 DFT-B3LYP 理论对非血红素铁超氧化物活化丙烯分子多态反应机理进行了探讨. 研究结果表明氢原子抽取过程遵守单态反应机制,主要在基态高自旋七重态势能面进行,且具有较低活化能($\Delta G^{\neq}$=65.6 kJ·mol^{-1}),非血红素铁超氧化物可以作为有效氧化剂抽取氢原子。单态反应机制可能归因于近来建议的交换–加强反应原则(EER,铁中心具有较大交换稳定作用)。对于 O-O 键的活化,在 CASSCF(10, 8)/6-31+G(d)//TZVP 水平下,势能面交叉区内,高自旋七重态(S_1)和五重态(Q_0)的自旋–轨道耦合(SOC)常数分别为 2.26 和 2.19 cm^{-1}。轨道分析表明两条发生翻转自旋轨道具有相同空间组成(π^*_{sub}),SOC 禁阻,因此通过 SOC 作用反应体系不可能有效地从七重态(S=3)势能面系间穿越到五重态(S=2)势能面,系间穿越可能发生在反应最后的退出阶段。

关键词: 非血红素铁超氧化物; 多态反应机理; 系间窜越; 自旋轨道耦合
中图分类号: O641.12+1 **文献标识码**: A **文章编号**: 1001-4861(2017)02-0329-11
DOI: 10.11862/CJIC.2017.028

Theoretical Investigation on the Multi-State Reaction Mechanism for the Propene Catalyzed by Non-Heme Ferric-Superoxo Species

LÜ Ling-Ling*,[1] ZHU Yuan-Cheng[1] ZUO Guo-Fang[1] YUAN Kun[1] WANG Yong-Cheng[2]
([1]*College of Chemical Engineering and Technology, Tianshui Normal University, TianShui, Gansu* 741001, *China*)
([2]*College of Chemistry and Chemical Engineering, Northwest Normal University, LanZhou*, 730070, *China*)

Abstract: The multi-state reaction mechanism for the propene catalyzed by non-heme ferric-superoxo model complex has been investigated at the DFT-B3LYP level. The calculations show that non-heme ferric-superoxo complex can be considered as effective oxidants in hydrogen atom abstraction reaction (single-state-reactivity), for which we find a lower barrier of $\Delta G^{\neq}$=65.6 kJ·mol^{-1} on the septet spin state surface. Single-state-reactivity is possibly due to the recently proposed exchange-enhanced reactivity (EER) principle with larger exchange stabilization of the Fe center. For the O-O bond activated step, we computed the spin-orbit coupling(SOC) constants of the septet, S_1 and quintet, Q_0 state at the crossing region and found it to be 2.26 and 2.19 cm^{-1} at the CASSCF (10, 8)/6-31+G (d)//TZVP levels, respectively. Orbital analysis show that two spin orbitals have the same spatial component in their wave functions (π^*_{sub}), therefore, the S=3 surface cannot effectively intersystem cross to the S=2 surface through the SOC interactions, and the intersystem crossing is possibly occurred at the exit stage of the reaction.

Keywords: non-heme ferric-superoxo; multi-state reaction mechanism; intersystem crossing; spin-orbit coupling

收稿日期:2016-02-04。收修改稿日期:2016-12-03。
国家自然基金(No.21263022;21663025;2163024)、甘肃省教育厅导师基金和天水师范学院“青蓝”人才工程基金资助项目。
*通信联系人。E-mail:lvling002@163.com

0 Introduction

Mononuclear non-heme Fe enzymes catalyze a diverse range of oxidation reactions, including hydroxylation, halogenation, ring closure, desaturation and electrophilic aromatic substrate that are important in medical, pharmaceutical, and environmental applications [1-2]. Several species including ferryl-oxo, ferric-superoxo, and ferric-peroxy have been proposed or found to act as oxidants in these enzymes [2]. However, our understanding of the non-heme ferric-superoxo complexes is rather scant, as opposed to the well studied oxy-heme species. Thus, mononuclear non-heme complexes in enzymes and synthetic analogues have attracted considerable interest recently. The lower-valent ferric-superoxo species have been directly observed in naphthalene dioxygenase (NDO) and homo-protoctaechute 2,3-dioxygenase (HPCD)[3]. Furthermore, synthetic ferric-superoxo and other metal-superoxo species were recently reported to be capable of catalyzing oxidation, including C-H bond activation [4]. Interestingly, compared with heme enzymes, many non-heme enzymes can use ferric-superoxo species as an oxidant but only a few heme enzymes (tryptophan 2,3-dioxygenase (TDO), and indoleamine 2,3-dioxygenase (IDO) so far) use ferric-superoxo species[5-6], which has also attracted our attention as a candidate for the active oxidant in the non-heme enzymes catalysis. Morokuma and co-workers compared reactivity of several vital ferryl-oxo and ferric-superoxo model complexes including title non-heme complex 1 model through DFT calculations to provide clues for rational design of ferric-superoxo oxidants[2], where it has been shown that a dominant feature of these reactions is the two-state reactivity (TSR) and multistate reactivity (MSR) that transpires due to the close proximity of the different multi-spin states in the ground state[7].

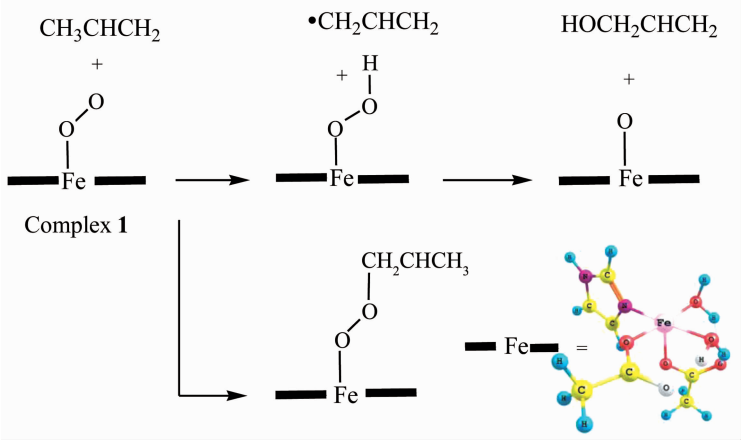

Scheme 1 A model reaction for the propene catalyzed by non-heme ferric-superoxo species

For ferric-superoxo complexes, the findings show that ferric-superoxo species can be converted to a ferryl-oxo complex via O-O bond cleavage, thus these species seem to share one common fundamental feature of the TSR/MSR mechanisms, they involve energy profiles of at least two spin states that either crossing or remain in proximity. Thus, the title reaction possibly occurs on two or more potential energy surfaces(PESs) under thermal conditions.

Therefore, detailed analyses of crossing seam between the different PESs are important in order to better understand the TSR/MSR mechanism of the propene catalyzed by non-heme ferric-superoxo species(Scheme 1). This kind of knowledge is essential for understanding the whole reaction mechanism and is useful for establishing an appropriate model for the O-O bond cleavage processes. To our knowledge, a deep theoretical study for the propene catalyzed by non-heme ferric-superoxo species has not been reported. However, since an experimental proof of mechanism is not a simple matter, in this sense, theoretical chemistry, specifically density functional

theory (DFT) has been playing an essential role in role in providing mechanistic data and structures of unstable intermediates and in deriving useful concepts. In the present paper we have performed hybrid DFT calculations on the reactions of the propene catalyzed by non-heme ferric-superoxo compound **1** models (Fig.1) to paint global pictures and discussed crossing seams, spin-orbit coupling (SOC) and possible spin-inversion processes in the O-O bond cleavage step.

1 Computational details

1.1 Geometrical optimization

Energies and geometries of the reaction intermediates and the transition states were calculated using the Gaussian 09 program package [8] and the unrestricted hybrid density functional UB3LYP with the 6-31+G(d) basis set[9]. The basis set used in DFT calculation for single point energies on final geometries is LACVP+* [10], which has been widely used for transition-metal-containing systems and has an effective potential that accounts for the scalar relativistic effects in iron. At the non-local functional UBP86 level, single-point energy calculations were performed using the LACVP+* basis set for all the atoms. The PCM approach for accounting solvent effects (single points with CH_3CN as solvent) was applied in the UBP86/LACVP+* level. However, UBP86 tended to overstabilize the low-spin ground state resulting in a large energy splitting between spin states, and in some cases this lead to an incorrect ground state (see Supporting Information). In addition, previous investigations of transition metal compounds employing the B3LYP functional by other groups[11] and us [12] indicated that this approach shows a very promising performance to predict properties such as bond dissociation energies, geometries, and harmonic frequencies with an accuracy comparable to that obtained from highly correlated wave function based ab initio methods.

1.2 Treatment of spin-orbit coupling

The SOC matrix elements are treated by an accurate multicenter mean-field (RI-SOMF) approximation[13-15] with the reasonable complete active space self-consistent field, CASSCF (10, 8) (ten activate electrons occupy the eight metal-ligand activate orbitals). An efficient implementation of the SOMF concept was explained, which is based on the following formulation of the effective one-electron operator[16]:

$$\begin{aligned}\langle\varphi_\mu|\hat{h}_k^{\mathrm{SOC}}|\varphi_\nu\rangle = \langle\varphi_\mu|\hat{h}_k^{\mathrm{1el\text{-}SOC}}|\varphi_\nu\rangle + \\ \sum_{k\tau} P_{k\tau}[(\varphi_\mu\varphi_\nu|\hat{h}_k^{\mathrm{2el\text{-}SOC}}|\varphi_\kappa\varphi_\tau) - \\ 3/2(\varphi_\mu\varphi_\kappa|\hat{h}_k^{\mathrm{2el\text{-}SOC}}|\varphi_\tau\varphi_\kappa) - \\ 3/2(\varphi_\tau\varphi_\nu|\hat{h}_k^{\mathrm{2el\text{-}SOC}}|\varphi_\mu\varphi_\kappa)]\end{aligned} \quad (\mathbf{1})$$

$$\hat{h}_k^{\mathrm{1el\text{-}SOC}}(r_i) = \frac{\alpha^2}{2}\sum_i\sum_{\mathrm{A}} Z_{\mathrm{A}} r_{i\mathrm{A}}^{-3} I_{i\mathrm{A};k} \quad (\mathbf{2})$$

$$\hat{h}_k^{\mathrm{2el\text{-}SOC}}(r_i, r_j) = -\frac{\alpha^2}{2} I_{ij;k} r_{ij}^{-3} \quad (\mathbf{3})$$

In Eq.**1**, the first term $\langle\varphi_\mu|\hat{h}_k^{\mathrm{SOC}}|\varphi_\nu\rangle$ is the one-electron term of the SOMF approximation, and the two-electron part (the first term in the summation) features a Coulomb term, which is efficiently and accurately represented by the resolution of the identity (RI) approximation, while the last two in the summation are much smaller exchange terms in Eq.**1**., which are sufficiently well treated within a one-center approximation. These operators explicitly take care of the one- and two-electron parts of the Breit-Pauli SOC operator[17] and includes the spin-same-orbit (SSO) as well as spin-other-orbit (SOO) terms in its two-electron part. As for parameters of Eqs.**2** and **3**, Z_{A} is the nuclear charge of atom A, $r_{i\mathrm{A}}$ is the position of the i'th electron relative to nucleus A, and $I_{i\mathrm{A};k}$ is the k'th component of the angular momentum of the i'th electron relative to atom A. Likewise, $I_{ij;k}$ is the k'th component of the angular momentum of electron i relative to electron j. These calculations were performed with a development version of the ORCA 2.8 program[18].

2 Results and discussion

2.1 Electronic structures of ferric-superoxo species

The optimized geometries and energetic data for the septet, quintet, and triplet electronic states are

depicted in Fig.1 and Table S1 (Supporting information), respectively. In order to keep the discussion more simple, the goal complex, denoted as $^{7(5)}1_{side\text{-}on}$ or $^{7(5)[3]}1_{end\text{-}on}$, is initially formed as Fe center and O_2 collide side-on or end-on with each other, where the superscripts denote the spin multiplicities. Compared to the reaction mechanism, side-on complex, $^{7(5)}1_{side\text{-}on}$ is not an important point discussed.

We obtain a septet $^{7}1_{end\text{-}on}$ complex, wherein O_2 is bound end-on and is an Fe(Ⅲ)-superoxo complex. The electronic structure of $^{7}1_{end\text{-}on}$ is in detailed shown in Fig.2. From Fig.2, O_2 here is a superoxide, having a singly occupied $\pi^*_{\perp}$, which is perpendicular to the Fe-O-O plane, while the other doubly occupied π^* orbital, $\pi^*_{//}$ in the Fe-O-O plane, forms a 3-e bond with the Fe d_{z^2} orbital. In other words, in the plane $\pi^*_{//}$ orbital of the superoxo interacts with the d_{z^2} orbital of the Fe in a π-type fashion, which leads to forming two new orbitals $d_{z^2}\pm\pi^*$, as shown in Fig.2. Thus, the septet $^{7}1_{end\text{-}on}$ will involve ferromagnetic coupling of S=5/2 Fe(Ⅲ) with the S=1/2 superoxo anion O_2^-.

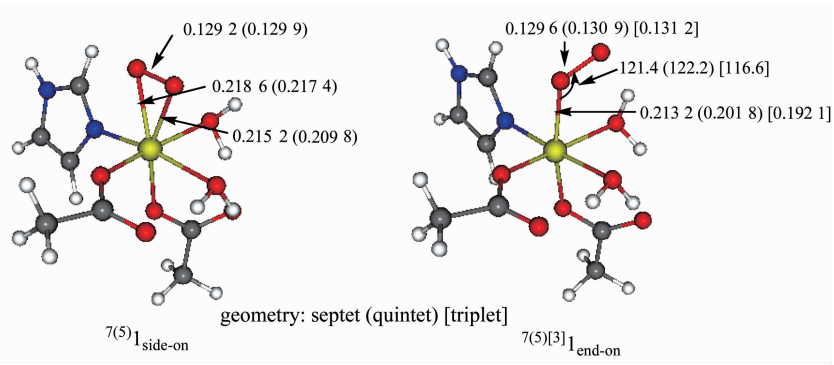

Data are given for septet (quintet) [triplet] states, respectively. Bond lengths are in angstroms

Fig.1 Optimized geometries of the different spin states non-heme Ferric-superoxo complexes at the UB3LYP/6-31+G(d) level

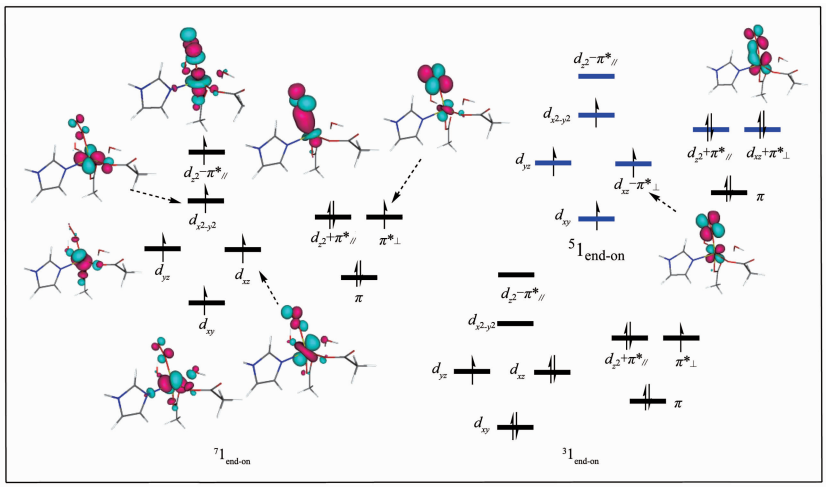

Fig.2 Electronic configurations of septet, quintet and triplet states of the end-on complex **1**

For the quintet $^{5}1_{end\text{-}on}$ complex, one character of $^{5}1_{end\text{-}on}$ is that its formal iron oxidation state can be assigned as Fe(Ⅳ)-peroxo. The reason is that the $\pi^*_{\perp}$ orbital of the O_2 moiety in $^{5}1_{end\text{-}on}$ is doubly occupied. Formally, there are four unpaired α electrons in $^{5}1_{end\text{-}on}$, spin density on Fe is 4.09. To identify some main atomic orbital interactions, the main antiferromagnetic orbital interactions were also inferred from overlaps calculated from the broken symmetry wave function (UB3LYP/6-31 +G (d)), the results calculated are plotted in Fig.3. Calculation results show that $d_{z^2}\pm\pi^*_{//}$ electrons are actually highly prone to spin

polarization, i.e., partial separation of α- and β-spin electrons in the $d_{z^2}\pm\pi^*_{//}$ orbital into spatially different regions, since electrons paired in orbital repel each other electrostatically. Restricted open-shell B3LYP calculations indeed show instability relative to broken-symmetry (BS) solutions. The overlap between d_{z^2} and $\pi^*_{//}$ is considerably better than the overlap of $\pi^*_{\perp}$ and any Fe3d orbital, and the overlap is $T=<d_{z^2}|\pi^*_{//}>=0.64$. The singlet coupling between d_{xz} and $\pi^*_{//}$ electron pair is therefore strong enough to lead to a short of the Fe-O distances (0.201 8 nm) in ^{5}1$_{end\text{-}on}$, as compared with that (0.213 2 nm) of ^{7}1$_{end\text{-}on}$.

As for ^{3}1$_{end\text{-}on}$, O_2 is bound end-on and is an Fe(Ⅲ)-superoxo complex, having a singly occupied $\pi^*_{\perp}$ orbital and a doubly occupied $\pi^*_{//}$ orbital. Then ^{3}1$_{end\text{-}on}$ involves ferromagnetic coupling of S=1/2 Fe(Ⅲ) with the S=1/2 superoxo anion O_2^-. Relative to ^{7}1$_{end\text{-}on}$, the DFT-calculated relative free energy of ^{3}1$_{end\text{-}on}$ is 48.9 and 51.8 kJ·mol^{-1} at the B3LYP/6-31 +G (d) and B3LYP/LACVP+* levels, respectively. Compared with the coupling of ^{5}1$_{end\text{-}on}$, the singlet coupling between $\pi^*_{//}$ and d_{z^2} in ^{3}1$_{end\text{-}on}$ is much stronger, the overlap $T=<d_{z^2}|\pi^*_{//}>\approx 1$ with the covalent interaction, which will lead to decrease the distance of Fe-O bond (0.192 1 nm).

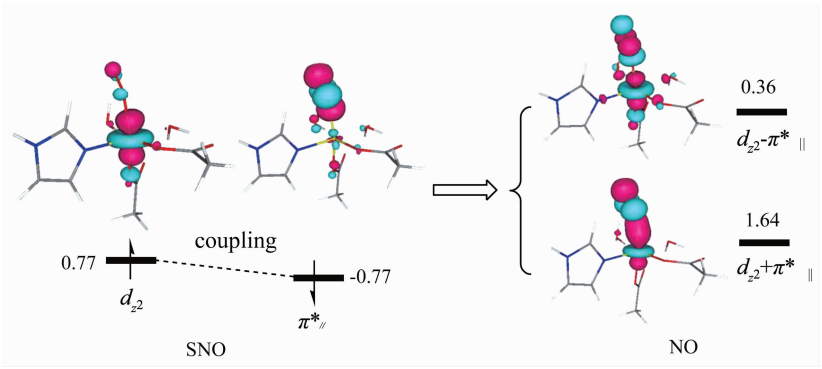

Occupancy numbers are marked

Fig.3　Spin natural orbitals (SNO) and natural orbitals (NO) obtained with the symmetry broken method in ^{5}1$_{end\text{-}on}$

2.2　Hydrogen-atom abstraction

The optimized geometries and relative energies in the triplet, quintet, and septet electronic states are shown in Fig.4 and Table S2 (Supporting information), respectively. The calculated potential energy profiles for the different spin states are shown in Fig.5. Initially, the three reactive states of $^{7(5)[3]}$1$_{end\text{-}on}$ form reactant complexes, $^{7(5)[3]}$R1, in which $^{7(5)[3]}$1$_{end\text{-}on}$ is weakly bound to propene. An electrophilic attack by a $^{7(5)[3]}$1$_{end\text{-}on}$ species is enabled through a σ-attack of the superoxo $\pi^*_{\perp}$ orbital. This leads to the transfer of a H-atom along with a spin-down electron from the C-H bond of the substrate into the $\pi^*_{\perp}$ orbital of O_2 to generate a ferric hydroperoxo product and a radical on substrate. Thus, a strong $\pi(O_2^-)$ bond is broken. Since the electron is transferred into the superoxo $\pi^*_{\perp}$ orbital, this requires an end-on approach of the C-H bond of the substrate relative to the Fe-O-O plane to ensure good orbital overlap.

As can be seen from Fig.5, the lower energy pathway of the H-abstraction process was occurred on the high-spin (HS) S=3 state PES. The transition state ^{7}TS$_H$ has calculated barrier heights of $\Delta E^{\neq}$=78.6 kJ·mol^{-1} and $\Delta G^{\neq}$=65.6 kJ·mol^{-1} relative to ^{7}R1. If electronic energies and free energies in the gas-phase are compared, the spin state ordering in the reactants and transition states remains the same. This indicates that the reaction will take place through single-state reactivity on the HS S=3 state potential surface only, which is compared with the behavior of nonheme and heme iron-oxo complexes where generally two- or multi-state reactivity modes are obtained on competing spin state surfaces. This difference is possibly due to the exchange stabilization of the Fe center during the H-abstraction.

Based on the recently proposed exchange-

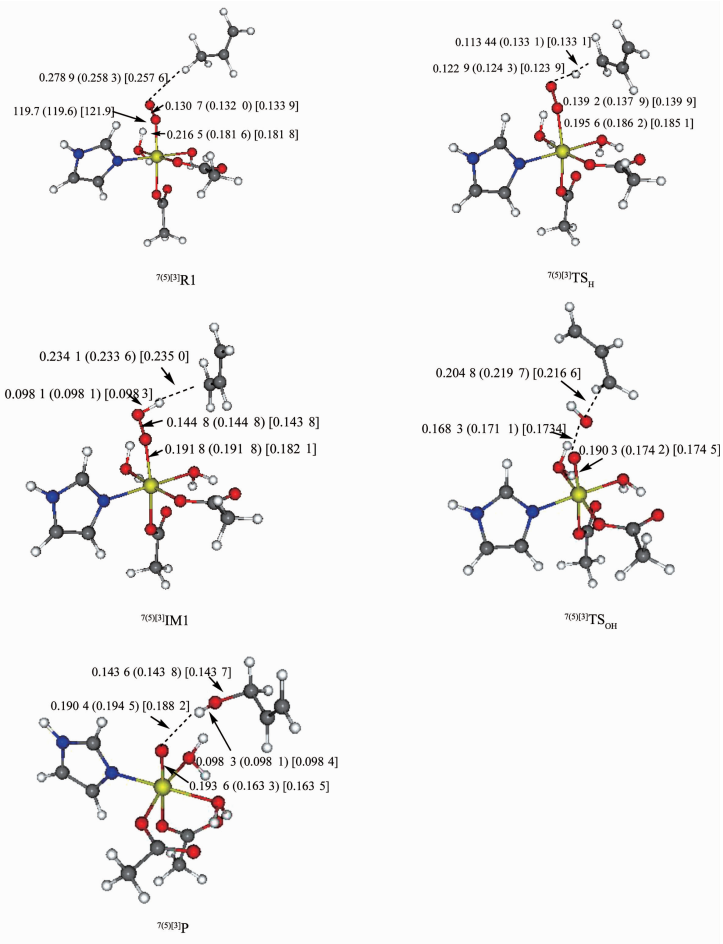

Data are given for septet (quintet) [triplet] states, respectively; Bond lengths are in nm

Fig.4 UB3LYP/6-31+G(d) optimized structures for the key species for the 2-propenol reactions of $^{7(5)[3]}1_{end\text{-}on}$ with propene

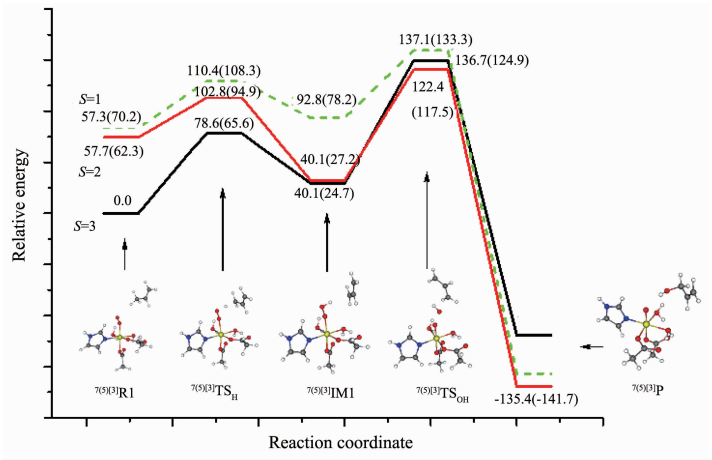

S=3, 2, and 1 refer to the spin states septet, quintet and triplet, respectively; Energies of parentheses given for ΔG

Fig.5 Energy profiles (in kJ·mol^{-1}) for the 2-propenol reactions of $^{7(5)[3]}1_{end\text{-}on}$ with propene. All energy values are at the UB3LYP/LACVP+* level

enhanced reactivity (EER) principle by Shaik et al[19], which states that if the number of identical-spin unpaired electrons on the metal center increases in the transition state (or the orbitals get more localized

on the metal center), this will maximize the exchange stabilization of the transition state. For the S=3, S=2, and S =1 spin states, during the H-abstraction, an electron shifts from the C-H bond to the O_2 $\pi^*_\perp$ orbital and thereby the d electron is freed from its antiferromagnetic coupling. *i.e.*, the number of unpaired d electrons of the Fe center is the same from reactants to ferric hydroperoxo intermediate. Therefore, the condition of the smaller deformation energy of the reactants on the spin state, the HS S=5/2 state has a lower barrier as compared with the low-spin (LS) states, leading to single-state reactivity. The suggestion that the HS S=5/2 iron center of all these electronic structures has a high reactivity due EER is consistent with the experimental results of the key role of the HS non-heme iron center in O_2 activation.

2.3 Calculations of O-O bond cleavage process

2.3.1 Crossing of the different PESs.

From Fig.5, the ground state product in quintet state, ^{5}P, will be formed from the intermediate in septet state, ^{7}IM1 via the transition state with the O-O bond broken. Therefore, at least a crossing and spin inversion process may be take place in the O-O cleavage reaction pathway. The geometric structure of the HS S =3 transition state, $^7TS_{OH}$ is very different from those of the intermediate spin (IS) S=2, $^5TS_{OH}$ and LS S=1, $^3TS_{OH}$ transition states (Fig.4). The $^7TS_{OH}$ has an O-O bond of 0.168 3 nm, which is shorter than those of the $^5TS_{OH}$, and $^3TS_{OH}$ (0.1711, and 0.173 4 nm, respectively). These bond lengths indicate the $^7TS_{OH}$ occurs early in the O-O bond cleavage coordinate. As the O-O bond distance increases, the HS S =3 potential energy surface steeply increases in energy and the S=2 potential energy surface gradually increases, which will lead to the crossing of different spin surfaces.

It is noted that the likelihood of such a crossover seems significant in view of the fact that the spin state surfaces are so close and cross from ^{7}IM1 to the crossing region (Fig.5). And, the ^{7}IM1 - ^{5}IM1 energy gap is very small (Fig.5). As such, a change in the geometry of the septet complex ^{7}IM1 in the direction of the quintet complex geometry, ^{5}IM1, causes crossing between the two states. Thereafter, the reaction can proceed on the quintet surface or bifurcate again to the septet surface. These will

Table 1　Contributions to the calculated ZFS between SOC and Spin-Spin (SS)(all numbers are in cm^{-1}) in the crossing region

Contributions		CASSCF(10,8) / 6-31+G(d)			CASSCF(10,8) / TZVP		
		x	y	z	x	y	z	
SOC	D(0)	−0.099	−0.202	−0.193	−0.107	−0.217	−0.207	
	D(−1)	0.000	0.000	0.000	0.000	0.000	0.000	
	D(+1)	0.000	0.001	0.001	0.000	0.001	0.001	
	total		0.247			0.265		
SS	Coulomb		0.118			0.124		
	Exchange		−0.019			−0.023		
	total		0.098			0.101		

Table 2　Calculated SOC matrix elements (cm^{-1}) of septet and quintet states in the crossing region by CASSC (10, 8) method

Basis stets	Septet	Quintet			
6-31+G(d)	S1	Q0	0.17	1.61	−1.57
		Q1	−89.82	−535.66	576.37
		Q2	507.77	−469.34	−379.17
TZVP	S1	Q0	0.16	1.56	−1.53
		Q1	95.69	563.72	−607.17
		Q2	−535.07	493.07	398.66

depend on the magnitude of the transition probability. Among the factors that affect the magnitude of the transition probability is the SOC interaction between the states. Let us then discuss the SOC interaction.

2.2.2 Spin-orbit coulping (SOC) in the crossing region.

Because of the intricate interplay of the spin-spin (SS) dipolar interaction with the SOC of the quintet state in the crossing seam, here we considered it desirable to include the calculation of zero-field splitting (ZFS) parameters (D-tensor, $D=D_{zz}-1/2\,(D_{xx}+D_{yy})$) [20]. The ZFS and SOC matrix elements were evaluated at the CASSCF (10, 8) wave function with 6-31+G(d) and TZVP basis sets using quasi-degenerate perturbation theory. These calculations were performed with the program ORCA 2.8[18]. The mixing of the S=3 and S=2 levels in the crossing seam by the spin-dependent terms in the Hamiltonian is treated approximately. Only the elements of SOC operator between the lowest HS septet state and the lowest three quintets are considered, where elements between quintets and triplets are ignored. These detailed results of the ZFS calculations are shown in Table 1. From the results in Table 1, the main contribution is from the second-order SOC interaction, while the SS contributions are negligible. The SOC part contains three parts: the SOC of electronic excited states of the same spin ($S_{excited}=S_{ground}$; $\Delta S=0$, $D^{(0)}$) into the ground state; from states differing by one spin flip ($S_{excited}=S_{ground}\pm1$; $\Delta S=-1$, $D^{(-1)}$ and $\Delta S=+1$, $D^{(+1)}$); and the elements of quintets, $S=2\rightarrow$ triplets, $S=1$ ($S=-1$), which are ignored($D^{(-1)}=0.0$). The $\Delta S=0$ contribu-tions are found to make significant contributions to $D_{xx}=-0.099$ cm^{-1}, $D_{yy}=-0.202$ cm^{-1}, and $D_{zz}=-0.193$ cm^{-1}, with the main contribution arising from the same spin states (i.e., the quintet ground state → excited quintet mixing). In addition, it is very small that the SOC contributions come from the spin-raising $\Delta S=+1$ excitations corresponding to the quintet ground state septet mixing, which indicates that the quintet and septet mixing can be forbidden by the SOC interaction.

In order to further understand the mechanism of intersystem crossing from the septet state to quintet state PES, the ROHF orbitals for the construction of the quintet and septet CASCI wave functions to be used in the SOC evaluation have been generated in the crossing region by quintet ROHF calculations, which were performed with the GAMESS program package[21]. At least eight active orbitals, as given in Fig.6 (in order to save space, the two nonactive doubly occupied orbitals are omitted), are found to be essential to reproduce the qualitative trends of SOC in the O-O bond cleavage step. The SOC matrix elements between the septet state and the quintet states in the crossing region are indicated in Table 2, we computed the SOC constants of the sextet, S_1 and quintet, Q_0

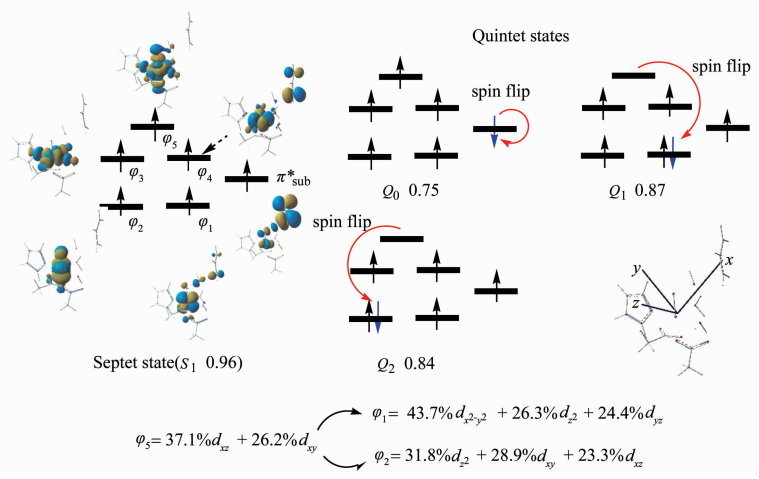

Fig.6 Electronic configurations of the SOC interactions of the septet state and quintet states (Q_0, Q_1 and Q_2) in the vicinity of the S_1/Q_0 crossing region for the O-O bond breaking step. The labels S and Q refer to the spin states septet and quintet, respectively.

state at the crossing region and found it to be 2.26 and 2.19 cm^{-1} at the CASSCF(10, 8)/6-31+G(d)//TZVP levels, respectively. These values are very low and provide a first hint that intersystem crossing may be forbidden primarily for an electronic reason. For facile spin flip from the S=3 to S=2 surfaces, the crossing points are required to have similar geometries and energies. Moreover, the electronic configurations must be able to SOC. SOC is effectively a localized, single-center, one-electron operator and can be written as

$$\begin{aligned}&\langle\varphi_\mu\theta_\mu|L\cdot S|\varphi_\nu\theta_\nu\rangle = \langle\varphi_\mu|L_z|\varphi_\nu\rangle\langle\theta_\mu|S_z|\theta_\nu\rangle+\\&\quad 0.5\langle\varphi_\mu|L_+|\varphi_\nu\rangle\langle\theta_\mu|S_-|\theta_\nu\rangle+\\&\quad 0.5\langle\varphi_\mu|L_-|\varphi_\nu\rangle\langle\theta_\mu|S_+|\theta_\nu\rangle\end{aligned}$$

or

$$\begin{aligned}&=\langle\varphi_\mu|L_z|\varphi_\nu\rangle\langle\theta_\mu|S_z|\theta_\nu\rangle+\\&\quad\langle\varphi_\mu|L_x|\varphi_\nu\rangle\langle\theta_\mu|S_x|\theta_\nu\rangle+\\&\quad\langle\varphi_\mu|L_y|\varphi_\nu\rangle\langle\theta_\mu|S_y|\theta_\nu\rangle\end{aligned}\qquad(\mathbf{4})$$

where L is the orbital angular momentum operator, and S is the spin operator, while $L\cdot S=I$ is the angular momentum of electron (see formulations **2** and **3** in Computational details); the φ is the space part of the molecular orbital, θ the spin of the electron. The $L_+S_-+L_-S_+$ operator in Eq.**4** performs a spin-flip and this process is accompanied by a change in the orbital due to the L_+/L_- raising/lowering operator [22]. Therefore, two orbitals of opposite spins in SOC have to different spatial components. In addition, SOC is also feasible only if two microstates differ solely in the occupation of two orbitals with the same spin states or two microstates have the same M_s for the two different spin states and these two orbitals can couple through the L_z operator.

Orbital analysis on the SOC mechanism are listed in Fig.6, for both spin states, S_1 and Q_0, the Fe center remains HS ferric with strong bonding interaction with the O atom. Hence, the major difference in the electronic structure between the S=3 and S=2 spin states at the crossing point lies in the spin of electron residing in the singly occupied π^*_{sub}, with α for S=3 and β for S=2. Obviously, two spin orbitals have the same spatial component in their wave functions (π^*_{sub}). Therefore, the S =3 surface cannot effectively intersystem cross to the S=2 surface through the SOC interactions as the orbital angular momentum operators associated with SOC in Eq.**4** require a change in orbital occupation. Thus, the reaction system can still proceed on the S=3 surface.

We also explored the SOC interaction of the septet state and two low lying quintet excited states, Q_1 and Q_2, involving mostly Fe-3d excitations due to a transition metal complex where there are a number of near-degenerate states for close lying metal d-orbials. From Fig.6, because the SOC constant (ζ_{Fe}) is an order of magnitude greater than the SOC values for oxygen, it is a reasonable approximation to consider only the Fe contribution when discussing spin-orbit mixing with quintet states. Thus for the SOC matrix elements of S_1 and Q_1 can be written as[17,23]

$$\langle\mathrm{SOC}\rangle = \eta C_0 C_{Q_1}\sum_k \zeta_{Fe}\langle\varphi_5|L_{Fe,k}|\varphi_1\rangle\langle\theta_5|S_k|\theta_1\rangle$$

where η is the M_s-dependent weighing factor, and $\theta=\alpha$ and/or β . In this case, for the septet state, S_1, the fundamental open-shell configuration has one dominant coefficient, *i.e.* C_0 =0.96 1, while the coefficient for quintet state is C_{Q_1}=0.87. Thus, the Q_1 state is generated from the septet S_1 state by electron shifts from φ_5 to φ_1, lead to the d-atomic orbital matrix elements, $\langle d_{xz}|L_y|d_{x^2-y^2}+d_{z^2}\rangle$, $\langle d_{xy}|L_y|d_{yz}\rangle$ and $\langle d_{xz}|L_z|d_{yz}\rangle$, $\langle d_{xy}|L_z|d_{x^2-y^2}\rangle$. Based on transfer of d orbitals under the operator of $L_{x,y,z}$ operators, the former will generate a y component of the SOC, the latter will lead to z component of the angular momentum, which is consistent with the calculated SOC values of $\langle^7\varphi|h_y^{SO}|^5\varphi\rangle$= −535.66 cm^{-1} and $\langle^7\varphi|h_z^{SO}|^5\varphi\rangle$=576.37 cm^{-1} at CASSCF(10, 8)/6-31+G(d) level. Similarly, the Q_2 state originates from the septet S_1 state by electron shifts from φ_5 to φ_2, leading thereby to an x, y components of SOC with the $\langle d_{xy}|L_z|d_{xz}\rangle$ and $\langle d_{xy}|L_z|d_{x^2-y^2}\rangle$ elements, respectively. These calculated results show that the Q_1 and Q_2 states in crossing point will produce a significant one-center SOC interaction. Therefore, this can enhance the probability of intersystem crossing from the septet to the quintet state. However, these spin-flip pathways ($S_1\rightarrow Q_1$, $S_1\rightarrow Q_2$) are unfeasible because the excited crossing points have signifi-

cantly higher in energy than the S_1 state, Q_1 and Q_2 are approximately 56.2 and 64.2 kJ·mol^{-1} higher than the S_1 state at the CASSCF(10,8)/6-31+G(d), respectively. Thus, the O-O bond homolysis step should remain on the S=3 surface as the reaction proceeds, overcoming an activation free energy of 124.9 kJ·mol^{-1} (Fig.5), while the intersystem crossing is possibly occurred at the exit stage of the reaction.

To further understand mechanism of the $S_1 \rightarrow Q_0$ spin-flip, the corresponding splitting and population distributions of Zeeman sublevels of an S=2 species with an applied field B in the vicinity of the S_1/Q_0 crossing region can be seen in Fig.7. In zero magnetic field, the lowest quintet state Q_0 is split into three spin states with eigenfunctions $|Q_x>$, $|Q_y>$, and $|Q_z>$, with an energy splitting described by the parameter D. For splitting of Zeeman sublevels, the eigenfunctions of the quintet spin states are given by $|Q_{\pm 2}>$, $|Q_{\pm 1}>$, and $|Q_0>$ and can be related to those at zero field by mixing coefficients that depend on the strength and direction of the magnetic field. From Fig.7, three zero field sublevels Q_x, Q_y, and Q_z are selectively populated, and their relative populations are carried over to the high field energy levels, $Q_{\pm 2}$, $Q_{\pm 1}$, and Q_0, Q_y, and Q_z overpopulation and some population on the Q_x sublevel. The populations on Q_y, and Q_z levels are nearly equal, 1.17×10^{-1}, whereas that on Q_x is somewhat smaller, 1.16×10^{-1}. These different populations are mainly attributed to the SOC-ISC interactions ($<^7\varphi|h_x^{SO}|^5\varphi>$= 0.17, $<^7\varphi|h_y^{SO}|^5\varphi>$=1.61, $<^7\varphi|h_z^{SO}|^5\varphi>$= −1.57 cm^{-1}), but these populations are very small, which indicate that intersystem crossing from septet to quintet is low efficient in the crossing region.

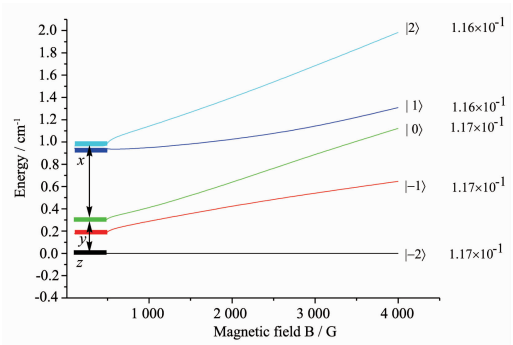

B is parallel to the z axis

Fig.7 Splitting and population distributions of Zeeman sublevels of an S=2 species with an applied field B in the vicinity of the S_1/Q_0 crossing region z axis of the molecule is defined as its Zeeman axis

3 Conclusions

In this study, the multi-state reaction mechanism for the propene catalyzed by non-heme ferric-superoxo model complex has been investigated using density functional theory calculations. For H-atom abstraction step, an electrophilic attack by a $^{7(5)[3]}1_{end\text{-}on}$ species is enabled through a σ-attack of the superoxo $\pi^*_{\perp}$ orbital. This leads to the transfer of a H-atom along with a spin-down β electron from the C-H bond of the substrate into the $\pi^*_{\perp}$ orbital of O_2 to generate a ferric hydroperoxo product and a radical on substrate. Thus, a strong $\pi(O_2^-)$ bond is broken. The lower energy pathway of the H-abstraction process was occurred on the HS S=3 state potential energy surface (PES). By contrast, the corresponding quintet and triplet H-abstraction barriers are well higher in energy and will not play a role of importance. These are possibly due to the exchange stabilization of the Fe center during the H-abstraction. As for the O-O bond broken step, at least a crossing and spin inversion process may be taken place in the O-O cleavage reaction pathway. In order to quantitatively understand the crossing of the S=3, S=2, and S=1 PESs, we computed the SOC constants (2.26 and 2.19 cm^{-1} at the CASSCF(10, 8)/6-31+G(d)//TZVP levels, respectively) of the septet, S_1 and quintet, Q_0 state at the crossing re-

gion. Orbital analysis show that the S=3 surface cannot effectively intersystem cross to the S=2 surface through the SOC interactions as the orbital angular momentum operators associated with SOC require a change in orbital occupation. Thus, the reaction system can still proceed on the S=3 surface.

Supporting information is available at http://www.wjhxxb.cn

References:

[1] Solomon E L, Brunold T C, Davis M I. *Chem. Rev*., **2010**, **100**:235-350

[2] (a)Nam W. *Acc. Chem. Res*., **2007**,**40**:522-531
(b)Chung L W, Li X, Hirao H, et al. *J. Am. Chem. Soc*., **2011**,**133**:20076-20079

[3] Mbughuni M M, Charkrabarti M, Hayden J A, et al. *Proc. Natl. Acad. Sci. U.S.A*., **2010**,**107**:16788-16793

[4] Peterson R L, Himes R A, Kotani H, et al. *J. Am. Chem. Soc*., **2011**,**133**:1702-1705

[5] Sugimoto H, Ods S L, Otsuki T. *Proc. Natl. Acad. Sci. U.S.A*., **2006**,**103**:2611-2616

[6] Li F, Meier K K, Cranswick M A, et al. *J. Am. Chem. Soc*., **2011**,**133**:7256-7259

[7] Hirao H, Kumar D, Que L, et al. *J. Am. Chem. Soc*., **2006**, **128**:8590-8606

[8] Frisch M J, Trucks G W, Schlegel H B, et al. *Gaussian* 09, Revision-D.01; Gaussian Inc.:Wallingford, CT, **2009**.

[9] Ditchfield R, Hehre W J, Pople J. A. *J. Chem. Phys*., **1971**, **54**:724-732

[10]Hay J P, Wadt W R. *J. Chem. Phys*., **1985**,**82**:299-309

[11]Lai W Z, Li C S, Chen H, et al. *Angew. Chem., Int. Ed*., **2012**,**51**:5556-5578

[12](a)LÜ Ling-Ling(吕玲玲), ZHU Yuan-Cheng(朱元成), WANG Xiao-Fang(王小芳). et al. *Chin. Sci. Bull*., **2013**,**58**:627-633
(b)Lü L L, Wang Y C, Wang Q. *J. Phys. Chem. C*, **2010**, **114**:17610-17620

[13]Sinnecker S, Neese F. *J. Phys. Chem. A*, **2006**,**110**:12267-12275

[14]Neese F, Edward I, Solomon E I. *Inorg. Chem*., **1998**,**37**: 6568-6582.

[15]Hess B A, Marian C M, Wahlgren U, et al. *Chem. Phys. Lett*., **1996**,**251**:365-371

[16]Neese F. *J. Am. Chem. Soc*., **2006**,**128**:10213-10222

[17]Danovich D, Shaik S. *J. Am. Chem. Soc*., **1997**,**119**:1773-17786

[18]Neese F. ORCA-an *ab initio*, *Density Functional and Semiempirical Program Package*, *Version* 2.8, Max-Planck Institute for Bioinorganic Chemistry, Germany, **2010**.

[19](a)Shaik S, Chen H, Janardanan D. *Nat. Chem*., **2011**,**3**: 19-27
(b)Mas-Ballesté R, McDonald A R, Reed D, et al. *Chem. Eur. J*., **2012**,**18**:11747-11760

[20]LÜ Ling-Ling(吕玲玲), WANG Xiao-Fang(王小芳), ZHU Yuan-Cheng(朱元成). et al. *Chin. Sci. Bull.* (科学通报), **2014**,**59**:286-296

[21]Granovsky A A. *GAMESS Program*, Moscow State University, Russia, **2007**.

[22]Pau M Y M. *Proc. Natl. Acad. Sci. U.S.A*., **2007**,**104**:18355-18362

[23](a)LÜ Ling-Ling(吕玲玲), WANG Xiao-Fang(王小芳), ZHU Yuan-Cheng(朱元成). et al. *Sci. China*: *Chem*.(中国科学:化学), **2012**,**55**:158-166
(b)LÜ Ling-Ling(吕玲玲), WANG Xiao-Fang(王小芳), ZHU Yuan-Cheng(朱元成). et al. *Acta Phys.-Chim. Sin*.(物理化学学报), **2013**,**29**:1673-1680